# Two-Dimensional Rare Gas Solids

ROBERT J. BIRGENEAU AND PAUL M. HORN

**Monolayers of rare gas atoms adsorbed onto the basal planes of graphite play the same prototype role in two dimensions that rare gas liquids and solids do in three dimensions. In recent experiments such novel phenomena as continuous melting, the lack of true crystallinity in two dimensions, orientationally ordered fluid phases, and melting from a solid to a reentrant fluid with decreasing temperature have been observed. Because the forces in these rare gas monolayers are simple and well understood, by studying them the investigator can examine a direct interface between experiment and first principles. In order to understand the phases and phase transitions that occur in such materials, it is necessary to consider the geometrical matching of the rare gas overlayer to the graphite substrate. It turns out that in two dimensions both the local and the long-distance behavior are important. These two-dimensional rare gas solids may be effectively probed with synchrotron x-ray techniques, and the results of a series of synchrotron x-ray scattering studies of these solids are presented.**

DURING THE PERIOD FROM 1894 TO 1898 THE RARE GASES helium, neon, argon, krypton, and xenon were discovered and isolated by Lord Rayleigh, W. Ramsay, and W. M. Travers (*1*). In fact, indirect evidence for the existence of the noble gases was contained in earlier measurements by Cavendish in 1784 (*2*). The condensed rare gases have been extensively studied for the last half century (*3*). Indeed, noble gas liquids and solids have been the traditional testing grounds for static and dynamic structural concepts in condensed-matter physics and chemistry. In virtually all elementary textbooks on liquids and solids, the first applications of concepts of binding, crystal structure, lattice dynamics, and liquid short-range order are made to condensed argon, krypton, and xenon.

This is so because the interactions are simple and well known. To a very good approximation, only forces between pairs of atoms need be considered. The interactions are spherically symmetric with a long-range van der Waals attractive term ($\sim r^{-6}$, where $r$ is distance) and a short-range repulsive term (conventionally taken to scale as $r^{-12}$). The magnitudes of the interactions may be deduced from gas-phase data. Thus first principles' calculations or computer simulations of such properties as the crystal structure, defect energies, and liquid short-range order are possible with essentially no adjustable parameters. Correspondingly, sophisticated measurements of these properties either in the liquid phase or in high-quality single crystals are possible. This has made possible a thorough development of our understanding of the properties of liquids and solids in three dimensions (*3*).

Since the pioneering theoretical work of Landau and Peierls (*4*) it has been known that the properties of solids in two dimensions should differ drastically from those in three dimensions. For example, Landau and Peierls demonstrated that crystalline order, as conventionally defined, cannot exist at any finite temperature in two dimensions. However, a more subtle form of translational order known as "topological order" may occur. Landau also recognized that, even if the translational long-range order did not exist, the crystalline axes could still be well defined; that is, one could have "bond-orientational" long-range order. This now turns out to be an important concept in both two- and three-dimensional systems. Much of the current interest in two-dimensional solids was stimulated as a result of a theoretical paper by Kosterlitz and Thouless (*5*). They predicted that freezing, which is always strongly first order in three dimensions, could occur continuously in two dimensions. Microscopically, this means that the positional order of the atoms in the fluid would grow continuously as the freezing transition was approached, reaching the size of the container at the freezing temperature (*5, 6*). This would be a very dramatic result, if indeed it did occur.

## Rare Gas Overlayers

The above discussion raises two questions: how does one prepare a model two-dimensional solid, and how does one probe the structure of such a solid with enough sensitivity to address the important issues? An answer to the first question has been known for some time. Thomy and Duval (*7*) in the late 1960's carried out accurate vapor pressure isotherm measurements of krypton and xenon physisorbed onto the basal planes of graphite. These measurements revealed that graphite could be prepared by exfoliation in a form with very high surface area (up to 80 $m^2/g$) with atomically flat basal planes extending over at least 1000 Å and with little alternate site adsorption. The rare gas atoms adsorb onto the surface, atomic layer by atomic layer, and the density on the surface may be controlled in equilibrium at the level of 1 percent of an atomic layer. Thomy and Duval obtained evidence for two-dimensional gas, liquid, and solid phases in the submonolayer coverage regime. From these data they deduced that the solid could be either in-registry or out-of-registry with the graphite substrate. They also observed transitions between these phases.

Important information about these surface structures has been obtained with the use of electron diffraction (*8, 9*), neutron scattering (*10*), and conventional x-ray diffraction (*11*) techniques. However, because the resolution of these techniques is limited, this inhibits study of the long-distance behavior and of the detailed evolution of the positional correlations at melting. The disadvantages of these probes are largely circumvented by the use of x-ray

R. J. Birgeneau is Cecil and Ida Green Professor of Physics at Massachusetts Institute of Technology, Cambridge, MA 02139. P. M. Horn is head of the Quantum and Statistical Physics Research Department at IBM T. J. Watson Research Center, Yorktown Heights, NY 10598.

synchrotron radiation (*12*). X-rays with both high intensity and excellent natural collimation are emitted from storage rings such as the Stanford Positron-Electron Asymmetric Ring (SPEAR) at the Stanford Synchrotron Radiation Laboratory (SSRL). The intensities and collimation are such that, with suitable instrumentation, one can obtain Bragg peak intensities of $\sim 10^6$ counts per minute from a single solid atomic layer (1 mm by 1 mm) of krypton with a resolution of 0.0001 $Å^{-1}$. This high resolution, which is unprecedented in surface science, allows one to probe the development of spatial order from the angstrom to the micrometer level. Accordingly, in 1980, together with D. E. Moncton, P. W. Stephens, and G. S. Brown, we began exploratory experiments at SSRL to study phase transitions in monolayer rare gas overlayers. Shortly thereafter, related experiments were initiated by J. Als-Nielsen, J. McTague, M. Nielsen, and J. Bohr at Deutsches Elekstronen-Synchrotron (DESY). We discuss here the science that has emerged from our experiments at SSRL, confining our attention to the behavior of krypton and xenon in the monolayer coverage range. Because of space limitations, other results will be discussed only to the extent that they are necessary for an understanding of the synchrotron experiments.

Many of the structural features of rare gas monolayers physically absorbed on graphite surfaces may be understood on the basis of simple energetic and geometrical considerations. The (001) basal plane of graphite with xenon and krypton atoms drawn to scale is illustrated in Fig. 1. The hierarchy of interactions is as follows. The largest energy is the uniform binding of the rare gas atom to the surface; this is equivalent to ~1400 K and ~1900 K for krypton and xenon, respectively. The next most important term is the adatom-adatom interaction; the simplest representation of this is the Lennard-Jones form

$$U = 4\epsilon \left[ \left(\frac{\sigma}{r}\right)^{12} - \left(\frac{\sigma}{r}\right)^{6} \right] \quad (1)$$

where $\epsilon$ is the pair interaction energy and $\sigma$ is the hard-core diameter (Fig. 1). From gas-phase data one deduces that for krypton $\sigma$ is ~3.65 Å and $\epsilon$ is ~163 K and for xenon $\sigma$ is ~3.98 Å and $\epsilon$ is ~232 K. Equation 1 is illustrated for xenon at the bottom of Fig. 1. The pair potential energy, $u$, is a minimum for $r_0 = 2^{1/6}\sigma$, and this gives approximately the equilibrium separation in the bulk solid. The final important energy is the corrugation of the surface potential. The preferred adsorption site for both krypton and xenon is the center of the graphite hexagon, whereas the least favorable configuration is one in which the rare gas atom is sitting directly on top of a carbon atom. However, the net difference in energy is only 40 to 80 K, much less than the overall binding energy.

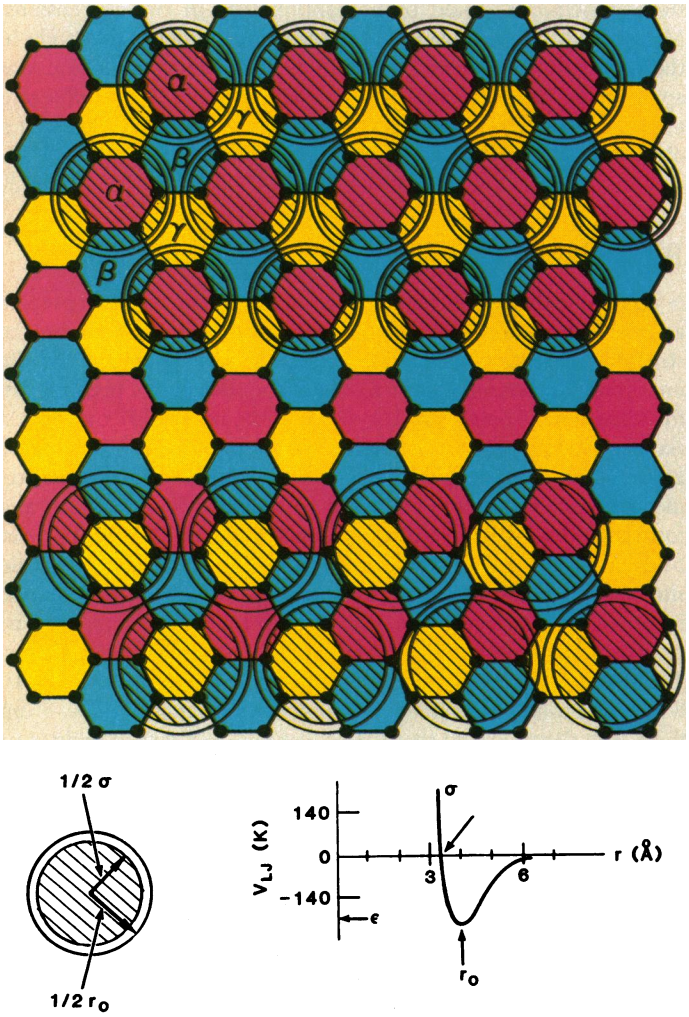


Fig. 1. Sketch of krypton (upper) and xenon (lower) on graphite drawn to scale showing explicitly the zero energy and minimum energy Lennard-Jones separations. The plot at the bottom right shows the Lennard-Jones energy as a function of separation for xenon.

Let us now consider the possible structures for submonolayer krypton and xenon on graphite. We begin with krypton, which is illustrated at the top of Fig. 1. The rare gas atoms prefer to sit in the center of the graphite hexagons. Krypton atoms are prevented from occupying neighboring hexagons by the strong short-range repulsive force. However, placement in next-nearest-neighbor hexagons gives a structure whose density is only ~10 percent smaller than ideal (Fig. 1). Since the periodicity of this structure is simply determined by the graphite, it is referred to as "commensurate." An essential feature of this structure is that there are three equivalent ways, labeled α, β, and γ and colored red, blue, and yellow, respectively, in Fig. 1, of placing the krypton atoms on the surface; α, β, and γ are referred to as "sublattices." The lattice vectors of the krypton unit cell are $\sqrt{3}$ longer than those of the underlying primitive cell of graphite and are rotated by 30° so that the structure is referred to as $\sqrt{3} \times \sqrt{3}$ R30°. An essential feature of commensurate overlayers is that they have discrete rather than continuous symmetry; this means that an infinitesimal displacement of all the krypton atoms costs a nonzero amount of energy. When one views Fig. 1, a question arises. Suppose all the $\sqrt{3} \times \sqrt{3}$ sites are filled. If one adds an extra krypton atom, will it go on the second layer or will the krypton atoms move out of the graphite minima to accommodate it on the first layer? We shall address this question in detail later in this article.

The xenon case is superficially more complicated. The graph at the bottom of Fig. 1 shows the xenon atoms packed at the Lennard-Jones equilibrium separation. It is evident that the lattice constant is slightly larger than the $\sqrt{3} \times \sqrt{3}$ value, and one obtains an incommensurate structure. Suppose one now holds the density fixed and moves the atoms to the center of the nearest hexagon. One then obtains locally the structure shown at the left in Fig. 2. The xenon atoms occupy one sublattice (say α) for some distance; however, since the $\sqrt{3} \times \sqrt{3}$ commensurate structure is denser than the xenon incommensurate structure, there must at some point be a vacant region; the xenon atoms then resume the $\sqrt{3} \times \sqrt{3}$ structure but occupy a second sublattice (say β). The vacant region is called an α-β domain wall or misfit dislocation. Depending on energetics, the domain walls themselves may form either a hexagonal array or a striped pattern. The site preference energy of the xenon atoms is, in fact, relatively small; thus an actual vacant region like that shown at the left of Fig. 2 is unlikely. Minimization of the temperature $T = 0$ energy for a periodic linear array of domain walls

yields the domain wall structure shown at the right in Fig. 2 (*9, 13*). The shift of the xenon atoms from one sublattice to the other occurs over a distance of six to eight xenon atoms.

This domain wall concept, first introduced by Frank and van der Merwe in 1949 (*14*), is essential for understanding the physics of surface overlayers and intercalation compounds as well. A full discussion of the statistical physics of domain walls is beyond the scope of this article. Here we note only several basic features. First, in the solid the domain walls that repel each other must themselves form a periodic lattice; the domain wall array may be hexagonal, preserving the underlying symmetry, or it may be linear, producing a rectangular or parallelepiped unit cell. Second, if the domain wall spacing is incommensurate with respect to the substrate, the overall structure is incommensurate even though most of the atoms might occupy graphite lattice sites. Third, entropic wandering of the domain walls plays an essential role in determining the total free energy of the overlayer.

Before presenting the experimental results, we need to introduce some additional theoretical concepts. In the 1930's, Landau and Peierls demonstrated (*4*) that one could not have true crystalline order in two-dimensional, continuous-symmetry systems, because the amplitude of vibration due to the long-wavelength elastic waves diverges logarithmically with the size of the sample. It turns out, however, that a state of matter may occur in which the positional correlations decay algebraically with distance. This algebraic decay state has a form of order called "topological order"; it has most of the properties of a normal solid, including crystalline axes that are perfectly well defined. The algebraic decay manifests itself in an interesting fashion in an x-ray diffraction experiment. In a three- or two-dimensional commensurate solid, the x-ray cross section is a sum of perfectly sharp Bragg peaks

$$S(\mathbf{Q}) \sim \sum_{\mathbf{G}} e^{-2W_{\mathbf{G}}}\, \delta\,(\mathbf{Q}-\mathbf{G}) \qquad (2)$$

where $\mathbf{Q}$ is the momentum transfer; $\mathbf{G}$ is a reciprocal lattice vector; and $\delta(\mathbf{Q}-\mathbf{G})$ is the Kronecker delta function, which equals 0 when $\mathbf{Q}-\mathbf{G}$ is non-zero and is infinite for $\mathbf{Q}-\mathbf{G}=0$; it has unit integral. This is the algebraic representation of the familiar Bragg spots in an x-ray diffraction pattern. The factor $e^{-2W_{\mathbf{G}}}$ is the Debye-Waller factor which depends on the atomic vibrations of the sample. For continuous-symmetry, two-dimensional systems, $W_{\mathbf{G}}$ diverges logarithmically with sample size with the consequence that Eq. 2 becomes

$$S(\mathbf{Q}) \sim \sum_{\mathbf{G}} |\,\mathbf{Q}-\mathbf{G}\,|^{-2+\eta_G} \qquad (3)$$

where

$$\eta_G = \frac{kTG^2}{4\pi K}$$

and $K$ is a combination of elastic constants. In the liquid state where information decays exponentially with distance, one might expect

$$S_p(\mathbf{Q}) = \sum_{\mathbf{G}} \frac{A}{\xi_p^{-2} + |\,\mathbf{Q}-\mathbf{G}\,|^2} \qquad (4)$$

where $\xi_p$ is the positional correlation length for the $G$th Fourier component of the mass density and $A$ is an amplitude.

Equation 4 implicitly assumes perfect bond-orientational order, which is not correct in the liquid state. Accordingly, we now consider the theoretical concept of bond-orientational order. In an ordinary fluid one can speak of two lengths, the positional correlation length $\xi_p$ of Eq. 4 and an orientational correlation length $\xi_6$ for triangular lattices. In an ordinary fluid, both are finite and equal to at most a few lattice spacings; the positional information decays exponentially over a length $\xi_p$; the orientation of the local axes

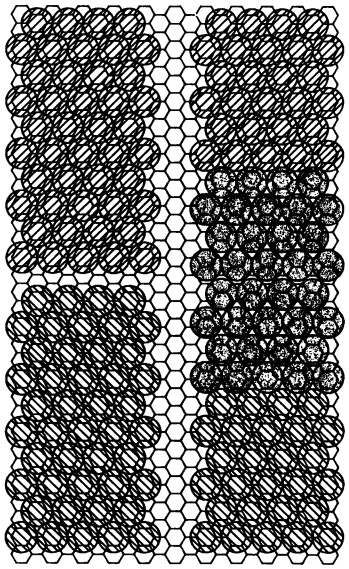

Fig. 2. (Left) Sharp superlight (two-thirds of a row of xenon atoms is missing) domain wall for xenon on graphite. (Right) Relaxed superlight domain wall. The shaded circles indicate xenon atoms whose positions deviate significantly from the commensurate position. [From Hong *et al.* (*13*)] A linear periodic array of such domain walls occurs below 65 K for a completed xenon monolayer.

becomes uncorrelated over a length $\xi_6$. It is possible to have a phase of matter, labeled "hexatic" for two-dimensional triangular lattices, in which $\xi_6$ is infinite; that is, the local axes are invariant across the sample, even though $\xi_p$ is finite. Such phases are common in three-dimensional liquid crystals (*15*), and they apparently also occur in quenched metallic glasses with fivefold symmetry (*16*). In an x-ray diffraction experiment, a fluid with both $\xi_p$ and $\xi_6$ finite will yield a ring of scattering with width in $|\,Q\,|$ of $\sim\xi_p^{-1}$.

The cross section for a hexatic fluid is more complicated. Even though $\xi_6$ is infinite, it is still possible to have local orientational fluctuations in the sample axes. Mathematically, one begins with Eq. 4 for the positional cross section and incorporates these fluctuations to first order by convolving Eq. 4 with, for example, a Lorentzian in the transverse direction

$$f(Q_\perp) = \frac{G\Delta\theta/\pi}{(G\Delta\theta)^2 + (Q_\perp - G_\perp)^2} \qquad (5)$$

where $\perp$ denotes the transverse direction and $\Delta\theta$ is the root-mean-square orientational fluctuation width in angle. As a consequence, the diffraction pattern will be a set of spots that are elliptical in shape with the orientational fluctuations manifesting themselves as an excess transverse width $G\Delta\theta$. This is illustrated at the left of Fig. 3. One of the most dramatic predictions of dislocation-mediated freezing theories (*5, 6*) is that the freezing should occur in two steps: from isotropic fluid to hexatic fluid and then from hexatic fluid to a solid with long-range orientational order and algebraic positional order; both transitions are predicted to be continuous.

With these concepts in hand, we can now proceed to discuss the synchrotron x-ray experiments.

## Synchrotron X-ray Experiments

It is immediately clear that in order to differentiate between ordinary Bragg scattering (Eq. 2), algebraic decay (Eq. 3), and a fluid with a long positional correlation length (Eqs. 4 and 5), we will need a probe that combines very high resolution with negligible multiple scattering so that line shapes can be interpreted quantitatively. The negligible multiple scattering criterion is satisfied by x-rays, which interact weakly with matter. The requirement for very high resolution may be met by the use of commercially available perfect silicon or germanium crystals as monochromator and analyzers; they act simultaneously as high-resolution collimators, giving a

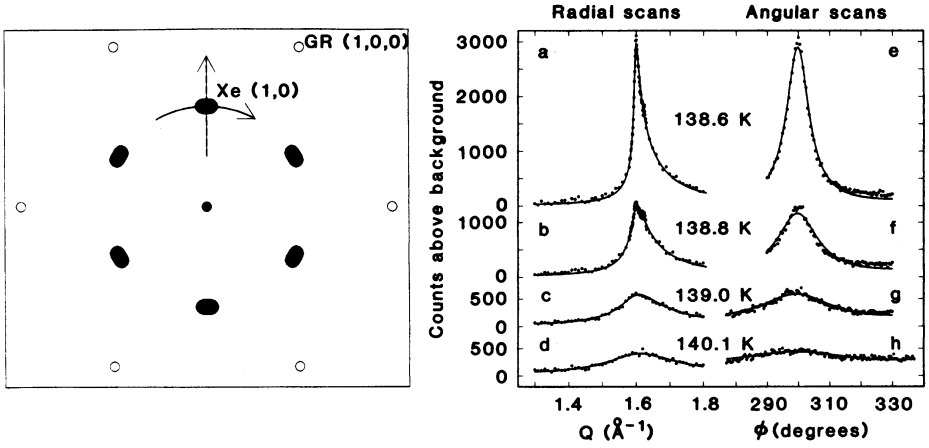


Fig. 3. (Left) Schematic of the intensity distribution in reciprocal space for a hexatic fluid with axes along the $\sqrt{3} \times \sqrt{3}$ R30° axes. (Right) Radial and angular scans through the xenon (1,0) peak in the fluid phase; the freezing temperature is 138.5 K; the solid lines are the results of fits to Eqs. 4 and 5 convoluted with the graphite (GR) mosaic and finite size functions. [Adapted from Nagler *et al.* (*21*)]

typical angular resolution of 15 seconds of arc. This translates into a real-space resolution of 10,000 Å or better. Unfortunately, at this resolution with a laboratory x-ray source the signal levels from surface overlayers are prohibitively small. This field of research has been made possible by the advent of x-ray synchrotron sources, which at high resolution provide ~$10^4$ times as many photons as the characteristic radiation from a rotating anode x-ray generator. Synchrotron radiation science has been discussed extensively (*9, 13*). For our purposes it is sufficient to regard the synchrotron beam line up to the x-ray diffractomator as a "black box" that provides a remarkably high flux of well-collimated, monochromatic x-ray radiation. We limit our discussion to two illustrative examples.

## Xenon on Graphite

The vapor pressure measurements of Thomy and Duval (*7*) strongly suggested that in the submonolayer coverage regime the two-dimensional xenon phase diagram is quite like its three-dimensional counterpart. It has a triple point structure with two-dimensional gas, liquid, and solid phases coexisting at $T_t$ = 99 K and triple-point coverage of ~0.8 monolayer. However, extrapolation of the Thomy-Duval liquid-solid coexistence boundaries to higher temperatures indicated to us that they could meet at 120 to 130 K and a coverage of ~0.9 monolayer, implying that the liquid-solid transition would be continuous for coverages greater than 0.9 monolayer.

High-resolution studies of the xenon monolayer melting based on the use of synchrotron radiation were first carried out by Heiney *et al.* (*17*) for a coverage of 1.1 monolayers; these measurements were extended to lower coverages by Dimon *et al.* (*18*). In both experiments a high-surface-area graphite substrate labeled UCAR ZYX was used. This substrate has extended flat graphite basal planes, ~2000 Å in extent, which are well aligned perpendicular to the basal planes but which form an azimuthal powder. Thus one can obtain accurate positional information, but the interesting orientational effects discussed above are lost in the two-dimensional powder average. The experiments of Heiney *et al.* (*17*) and Dimon *et al.* (*18*) present strong evidence for continuous freezing for coverages above 0.9 monolayer; here the coverage is in units of the areal density of the primitive cell at the phase boundary. Orientational information was first obtained in a rotating anode experiment at IBM by Rosenbaum *et al.* (*19*). They used as a substrate an exfoliated single crystal. The most precise experiments on the xenon submonolayer melting have been performed with the use of synchrotron radiation with both an exfoliated single crystal and a single crystal as substrates (*19–21*). We now discuss these results in detail.

As discussed above, in a fluid without bond-orientational order, the x-ray diffraction pattern should be a ring. However, if there is bond ordering, then the ring will condense into a series of elliptical spots centered about the ultimate Bragg positions (left of Fig. 3). We show at the right in Fig. 3 diffraction profiles of the first peak in the liquid structure factor of 1.0 monolayer of xenon on an exfoliated single crystal. These become the (1,0) peaks of the triangular lattice in the solid phase. The intrinsic angular spread (mosaicity) of the substrate is 3.2° half width at half maximum (HWHM), and the basal plane surfaces of graphite have a finite size of ~1400 Å. All these scans are in the fluid phase; the freezing temperature for this coverage is 138.5 K. All the profiles are broader than the resolution determined by the finite size and mosaicity of the substrate. On the scale of widths relevant to Fig. 3, the intrinsic synchrotron resolution is essentially perfect. It is evident that the diffraction profiles are just those expected from a bond–orientationally ordered fluid since an elliptical spot rather than a ring of scattering is observed. The angular scans are centered about the graphite $\sqrt{3} \times \sqrt{3}$ R30° axes so the fluid axes are aligned in that direction. As the freezing temperature is approached from above, both the radial and angular widths narrow progressively and ultimately take on the substrate values at $T \sim 138.5$ K. The aspect ratio (the ratio of angular width to radial width) of the liquid peaks is ~6 at these temperatures. The solid lines in Fig. 3 are the results of least-squares fits of Eq. 4 convoluted with Eq. 5 and the substrate resolution. From these fits one can extract the intrinsic radial and angular widths. These are shown in Fig. 4.

An experiment, similar to that of Nagler *et al.* (*21*) but with one single crystal used as a substrate, has been carried out by Specht *et al.* (*20*). For the single crystal the surface coherence length (the distance over which the surface is atomically flat and defect-free) was at least

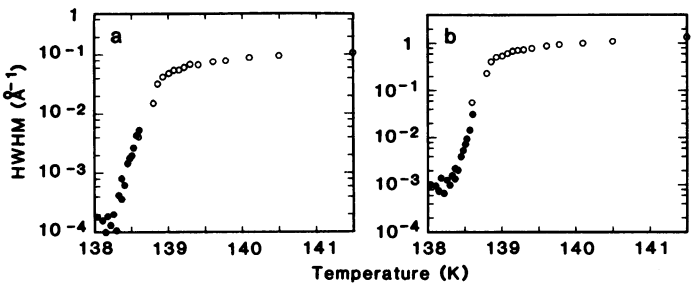


Fig. 4. Radial widths (a) and angular widths (b) in the fluid phase for ~1.0 monolayer of xenon on graphite; the open circles are for an exfoliated graphite substrate, the closed circles for one single crystal. The freezing temperature in the latter experiment has been increased by 5.0 K to permit superposition of the data. The data are from (*19–21*).

10,000 Å and the mosaicity was ~0.1°, so it was possible to obtain data in the fluid phase at much longer length scales. On the other hand, because of the small number of xenon atoms in the scattering volume, the signal became prohibitively small once the fluid positional correlation length was less than ~200 Å. By coincidence, this is the largest fluid length scale that could be probed in the exfoliated single-crystal graphite experiments. Thus the two substrates yield complementary information. The single crystal results are also shown in Fig. 4. The melting temperature $T_m$ of Specht *et al.* (*20*) has been increased by 5.0 K so that the data from the two experiments could be superimposed. This difference in $T_m$ corresponds to a difference in coverage of about 3 percent.

Figure 4 provides dramatic evidence for a continuous freezing transition in a two-dimensional solid, as originally predicted by Kosterlitz and Thouless (*5*). The value of $\xi_p$ reaches at least 2000 Å before the solid is entered. Furthermore, the ratio of the angular to the radial width is nearly constant throughout the fluid phase; the fluid thus always has a hexatic character. At the highest temperatures, the orientational order in the fluid undoubtedly is induced by the substrate although reasonable estimates of the relevant magnitudes suggest that $\xi_6 >> \xi_p$. What about the transition from isotropic to hexatic fluid predicted by Nelson and Halperin (*6*)? Here again, the data in Fig. 4 are consistent with an intrinsic hexatic phase near $T_m$ but they do not prove the existence of such a phase because the transition, if it occurs, is severely rounded by the substrate orienting field. These experiments provide definitive evidence for continuous, albeit very sharp, melting in two dimensions. They are consistent with the theories of Kosterlitz and Thouless (*5*), Nelson and Halperin (*6*), and Young (*6*), but they do not prove them uniquely.

## Krypton on Graphite

One of the most surprising features of the monolayer xenon-on-graphite system is that the substrate corrugation plays a minor role except at low temperatures. The most prominent effects are orientational rather than positional. From the geometrical considerations at the beginning of this article, one might expect more dramatic substrate effects for krypton. Early vapor pressure isotherm (*7*), electron diffraction (*8, 9*), and x-ray (*11*) measurements showed that this is indeed the case. For krypton we shall give all coverages in units of a complete $\sqrt{3} \times \sqrt{3}$ R30° monolayer. For coverages below ~1.0 monolayer, the structure is always the commensurate $\sqrt{3} \times \sqrt{3}$ R30° lattice shown at the top of Fig. 1 (*8, 9, 11*). The phase diagram is unusual, however, in that the triple point is eliminated and one has only fluid and solid phases. An elegant lattice gas model known as the "Pott-lattice-gas," which includes vacancies and possible occupancy of the α, β, and γ sublattices, has been proposed by Berker *et al.* (*22, 23*) for submonolayer krypton on graphite. By explicit calculation using known interaction constants, they have been able to explain quantitatively much of the submonolayer behavior.

Quite exotic behavior is observed in the coverage range between ~1.0 and ~2.0 layers, and we shall discuss those results in detail. The two-dimensional phase diagram determined by Specht *et al.* (*24*) for vapor pressures $P$ between 1 and 600 torr and $T$ between 114 and 134 K is shown in Fig. 5. It is most convenient to discuss this phase diagram in the context of the actual synchrotron x-ray data from which it was derived.

We show in Fig. 6 a series of synchrotron x-ray diffraction scans in the neighborhood of the (1,0) $\sqrt{3} \times \sqrt{3}$ commensurate position. In these experiments UCAR ZYX was used as the substrate, so again positional but not orientational information was obtained. The data

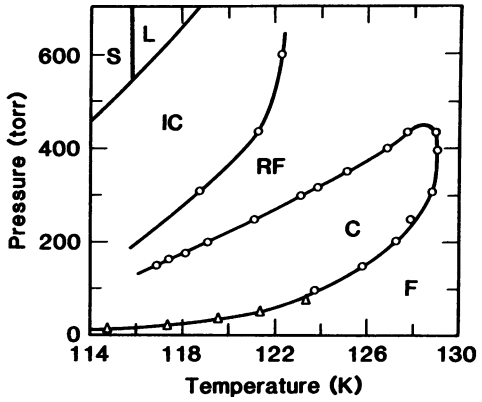


Fig. 5. Phase diagram of krypton on graphite exhibiting the fluid (F), $\sqrt{3} \times \sqrt{3}$ R30° commensurate (C), reentrant fluid (RF), and incommensurate solid (IC) phase. S and L represent the bulk solid and liquid phases, respectively. [From Specht *et al.* (*24*)]

in Fig. 6 were obtained by fixing the krypton $P$ at 310 torr and simply lowering $T$. The actual coverage on the surface for these data is not known precisely, although it is always in the vicinity of ~1.0 monolayer. Scans were carried out between $Q = 1.20$ Å$^{-1}$ and $Q = 2.20$ Å$^{-1}$ but only the center region is shown in Fig. 6. The graphite background has been subtracted so that only the krypton overlayer scattering is displayed. At 129.5 K, very broad scattering

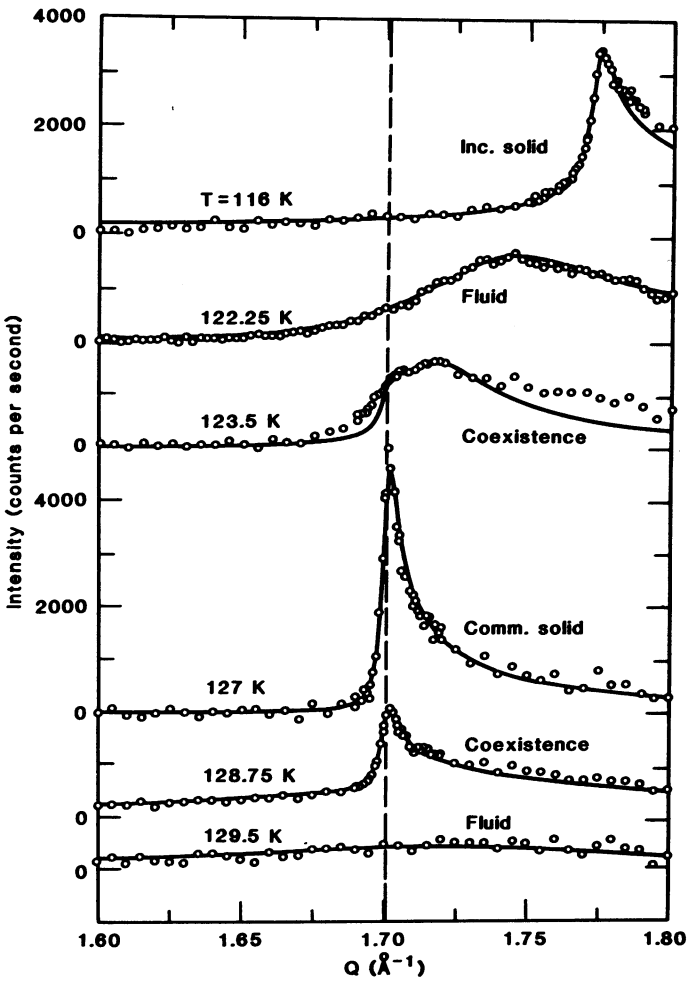


Fig. 6. Synchrotron x-ray scans in the neighborhood of the commensurate position (1.70 Å$^{-1}$) at a pressure of 310 torr. The solid lines are fits to Eqs. 2 through 5 as discussed in the text. [Adapted from Specht *et al.* (*24*)]

centered at the commensurate position is observed. The solid line, which is a fit to Eq. 4 circularly averaged, corresponds to $\xi_p = 16$ Å and $|G| \sim 1.70$ Å$^{-1}$. Thus at 129.5 K krypton forms a weakly correlated fluid with commensurate short-range order. When the temperature is lowered to 128.75 K, the liquid signal barely changes while a sharp peak appears at the (1,0) commensurate position. This is the signature of a first-order freezing transition from a weakly correlated fluid to a commensurate solid. By 127 K the fluid signal has vanished and the commensurate solid is fully developed. The solid line is a fit to a finite-size version of Eq. 2, that is, a Gaussian distribution with Lorentzian tails. The asymmetric line shape originates in the vertical mosaic of the UCAR ZYX substrate. As $T$ is lowered below 125 K, the solid peak begins to diminish and has virtually vanished by 123.5 K (Fig. 6). The diffraction profile at 123.5 K is best described as originating from a weakly incommensurate fluid with incommensurability $\epsilon = Q - Q_{comm} \sim 0.01$ Å$^{-1}$ and correlation length $\xi_p \sim 110$ Å. With further decreases in $T$ to 122.25 K, $\epsilon$ increases to 0.03 Å$^{-1}$ while $\xi_p$ decreases to 40 Å. The solid line at 122.25 K is a circularly averaged Lorentzian, Eq. 4; clearly this simple form describes the observed fluid structure factor quite well. With further decreases in $T$, $\xi_p$ increases and a continuous freezing transition occurs at ~119 K. The solid line at 116 K is the power law form, Eq. 3, with $\eta = 0.3$. The difference in the structure factor for discrete ($T = 127$ K) and continuous ($T = 116$ K) symmetry solids manifests itself dramatically in these data. Clearly, the phenomenon of melting with a decreasing $T$ evident in Figs. 5 and 6 is quite novel. Before discussing the probable underlying physics, we consider the experimental behavior at lower $T$.

The original discovery that a well-correlated fluid intervened between the commensurate and incommensurate solid phases for krypton on graphite was made by Moncton *et al.* (*25*) at $T = 97$ and 80 K. Thus the reentrant fluid phase evident in Fig. 6 extends far below the ordinary melting temperature. Their data (*25, 26*) also contained evidence for domain wall effects. The geometry of the domain walls for compressed krypton on graphite may be understood as follows.

If one takes a $\sqrt{3} \times \sqrt{3}$ krypton monolayer, contracts it so that the krypton atoms have about their Lennard-Jones separation, and then moves each krypton atom to the center of the nearest hexagon, one generates the lattice shown in the right inset of Fig. 7. It is evident that one produces a hexagonal network of domain walls; these particular walls have been denoted "super heavy" by Kardar and Berker (*22*). The explicit domain wall structure shown in Fig. 7 is not possible since the krypton atoms would have separations less then their hard-core values. Minimization of the total energy yields walls six to eight atoms wide (*27*), analogous to those for xenon shown in Fig. 2. If the domain walls themselves have long-range order, then one would now have a new, very long periodicity that would, in general, be incommensurate. The lowest order peaks that occur as a result of this new periodicity are illustrated in the right inset of Fig. 7; the primary peak is at $(Q_{comm}+\epsilon, 0)$, and the first-order satellite peaks occur at $(Q_{comm}-\epsilon, \epsilon)$ and $(Q_{comm}, -\epsilon)$.

Figure 7 shows diffraction scans in the fluid phase near the fluid-incommensurate solid boundary of both the primary peak and a satellite peak (*27*), based on the use of a single-crystal substrate at $T = 88.3$ K and $P \simeq 2$ torr. The annealed domain wall model predicts the relative intensities quite well. These data demonstrate that the superheavy domain wall concept is correct, that for $\epsilon \sim 0.04$ Å$^{-1}$ the domain walls are aligned along the axes shown in Fig. 7 and that at this $T$ and $P$ the domain wall network itself forms a well-correlated hexagonal fluid with a correlation length of ~400 Å. These data agree with the earlier UCAR ZXY results of Moncton *et al.* (*25*) and Stephens *et al.* (*26*) in the same $T$ range.

We thus have the novel empirical result that at small incommensurability, that is, when the domain walls are far apart, they form a fluid rather than a solid. With increasing $\epsilon$, the domain walls move together, interact more strongly, and then crystallize. This automatically explains the sequence $\sqrt{3} \times \sqrt{3}$ solid → weakly incommensurate fluid → incommensurate solid. The above explanation was in fact constructed on the spectrometer at SSRL by Moncton *et al.* (*25*) as the data were produced. It was understood at the time that the large entropy of the domain wall network must play an essential role, but the explicit mechanism for the domain wall disorder at weak incommensurability was not identified.

Since then, elegant theories for the phenomena have been given by Coppersmith *et al.* (*28*) and others (*22, 23*). The essential idea may be summarized as follows. The domain walls should be regarded as excitations that move freely in the lattice, bend and oscillate, but are not allowed to pass through each other. This has the consequence that the domain wall free energy is dominated by entropy. This domain wall disorder manifests itself dramatically in simulations by Abraham *et al.* (*29*) (Fig. 8). The domain walls are also seen to meander as a function of time in the simulations. The

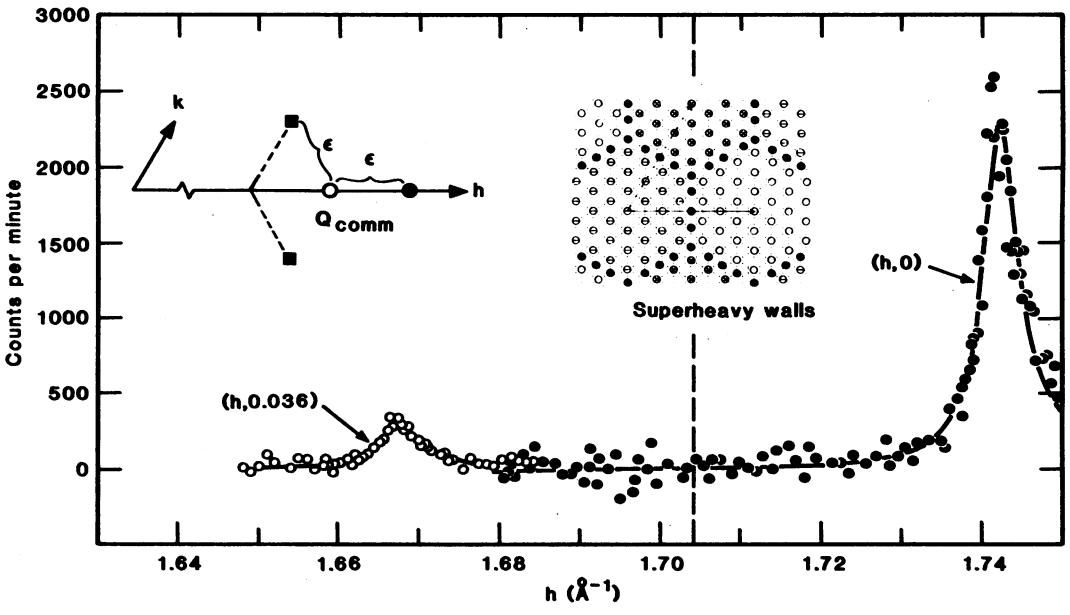


Fig. 7. Single diffraction scans through the primary ($h$, 0) and satellite ($h$, 0.036) krypton peaks at a temperature of 88.3 K and a pressure of 2 torr. [Data from D'Amico *et al.* (*27*)] The solid lines are fits to Lorentzians with $\xi_p = 400$ Å. The left inset shows the geometry in reciprocal space. The axes ($h$, $k$) are shown in the inset; $k$ is fixed at the specified values and $h$ is varied. The right inset shows a sharp superheavy domain wall configuration as discussed in the text.

energetics are such that the domain wall network is unstable to the formation of free dislocations (*28*). This is predicted to be true at all $T$ values for small incommensurabilities. A two-dimensional system with free dislocations is a fluid since it cannot sustain shear. Kardar and Berker and their colleagues (*22, 23*) have carried out a full microscopic lattice gas calculation including all possible domain walls as excitations. Their theory accounts rather well for the complete empirical phase diagram with only one adjustable parameter.

The unusual topology for the krypton phase diagram (Fig. 5) can be understood as follows. For coverages near ~2.0 monolayers, the close-packed incommensurate phase is favored. However, for coverages closer to ~1.0 monolayer, at high $T$ there is significant occupation of the second layer and there is also a significant number of krypton atoms in the vapor over the graphite. The second layer forms a dilute lattice gas while the structure of the depopulated first layer is commensurate. As $T$ decreases condensation occurs into the first layer from the second layer and from the vapor, thereby driving the commensurate-incommensurate transition. This commensurate-incommensurate transition is, in fact, a melting transition. This accounts for the reentrant character. Finally, the reentrant fluid freezes into an incommensurate solid.

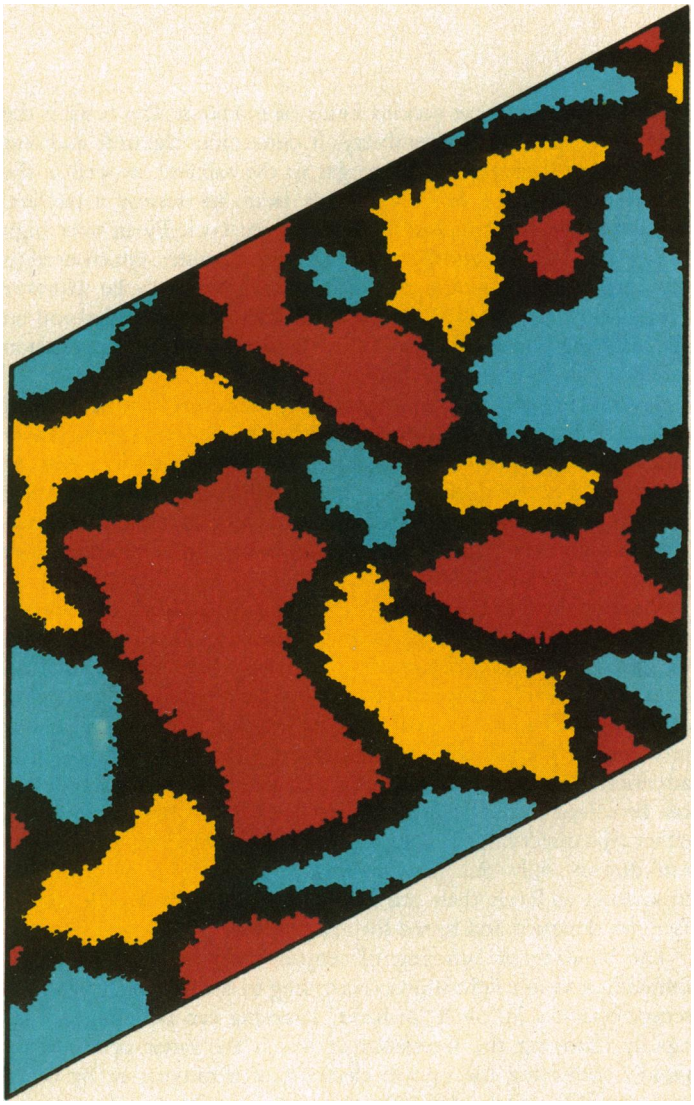

Fig. 8. A snapshot picture of the incommensurate krypton atoms (44%) for a 22,212 krypton atom system on graphite at a coverage of 1.05 monolayers, a temperature of 97.5 K, and a graphite linear dimension of 620 Å. The atomic configuration is for 20,000 time steps into the molecular dynamics simulation. The occupied substrate sublattices of the commensurate krypton atoms are color-coded to match those in Fig. 1. [Figure derived from data of Abraham *et al.* (*29*)]

## Final Comments

As these two examples illustrate, two-dimensional rare gas solids exhibit remarkably rich and interesting behavior with new phenomena unique to two dimensions. Synchrotron radiation has played, and will continue to play, an essential role in elucidating the fundamental behavior (i) because it opens up the distance scale between 100 and 10,000 Å and (ii) because the detailed line-shape analysis it allows can yield reliable information about the relevant correlation functions. The simplicity of the rare gases has allowed for straight-forward intuitive considerations as well as explicit microscopic calculations, just as for three-dimensional rare gas solids.

Concepts developed for three-dimensional rare gas solids have proven to be important throughout solid-state physics (*3*). It is legitimate to ask whether the same will hold true in two dimensions. Currently, much less is known about other two-dimensional solids. However, it is clear that the domain wall concepts discussed here can be applied directly to metal overlayers on metals and semiconductors. The concepts have already been applied to explain the in-plane behavior of intercalation materials. Experiments that are now under way on rare gas layer-by-layer crystal growth should also have broad consequences. Finally, new tools such as inelastic atom beam scattering are now being applied to rare gas monolayers and bilayers so that more detailed information about the excitations as well as the structures will become available. We expect, therefore, that two-dimensional rare gas solids will continue to be an active and productive area of research.


REFERENCES AND NOTES

1. Lord Rayleigh and W. Ramsay, *Philos. Trans. R. Soc. London Ser. A* **186**, 187 (1895); W. M. Travers, *Discovery of the Rare Gases* (Arnold, London, 1928).
2. H. Cavendish, *Philos. Trans. R. Soc. London* **74**, 119 (1784).
3. M. L. Klein and J. A. Venables, Eds., *Rare Gas Solids* (Academic Press, London, 1977), vols. 1 and 2; see especially G. Horton, *ibid.*, vol. 1, pp. 1–121.
4. R. E. Peierls, *Helv. Phys. Acta Suppl.* **7** (No. 11), 81 (1934); L. D. Landau, in *Collected Papers of L. D. Landau*, D. Ter Haar, Ed. (Gordon and Breach, New York, 1965), pp. 201–220; ——— and E. M. Lifshitz, *Statistical Physics* (Addison-Wesley, Reading, MA, 1969), pp. 401–404.
5. J. M. Kosterlitz and D. J. Thouless, *J. Phys. C* **6**, 1181 (1973).
6. D. R. Nelson and B. I. Halperin, *Phys. Rev. B* **19**, 2456 (1979); A. P. Young, *ibid.*, p. 1855.
7. See, for example, A. Thomy and Y. Duval, *J. Chim. Phys. Phys. Chim. Biol.* **66**, 1966 (1969); *ibid.* **67**, 286 (1970); *ibid.* p. 1101; *ibid.* **74**, 926 (1977); J. G. Dash, *Films on Solid Surfaces* (Academic Press, New York, 1975).
8. M. D. Chinn and S. C. Fain, Jr., *Phys. Rev. Lett.* **39**, 146 (1977).
9. P. S. Schabes-Retchkiman and J. A. Venables, *Surf. Sci.* **105**, 536 (1981).
10. H. Taub, K. Carneiro, J. K. Kjems, L. Passell, J. P. McTague, *Phys. Rev. B* **16**, 4551 (1977).
11. P. M. Horn, R. J. Birgeneau, P. A. Heiney, E. M. Hammonds, *Phys. Rev. Lett.* **41**, 961 (1978); P. W. Stephens, P. A. Heiney, R. J. Birgeneau, P. M. Horn, *ibid.* **43**, 47 (1979).
12. P. Eisenberger and L. C. Feldman, *Science* **214**, 300 (1981); D. E. Moncton and G. S. Brown, *Nucl. Instrum. Methods* **208**, 579 (1983); P. Eisenberger, *Science* **231**, 687 (1986).
13. Hawoong Hong, M. Sutton, R. J. Birgeneau, *Phys. Rev. B* **33**, 3344 (1985).
14. F. C. Frank and J. H. van der Merwe, *Proc. Soc. London Ser. A* **198**, 205 (1949); *ibid.*, p. 216.
15. R. J. Birgeneau and J. D. Litster, *J. Phys. (Paris) Lett.* **39**, 1399 (1978); R. Pindak, D. E. Moncton, S. C. Davey, J. W. Goodby, *Phys. Rev. Lett.* **46**, 1135 (1981).
16. P. A. Bancel, P. A. Heiney, P. W. Stephens, A. I. Goldman, P. M. Horn, *Phys. Rev. Lett.* **54**, 2422 (1985); M. V. Jaric, *ibid.* **55**, 607 (1985).
17. P. A. Heiney *et al.*, *ibid.* **48**, 104 (1982).
18. P. Dimon, P. M. Horn, M. Sutton, R. J. Birgeneau, D. E. Moncton, *Phys. Rev. B* **31**, 437 (1985).
19. T. F. Rosenbaum, S. E. Nagler, P. M. Horn, R. Clarke, *Phys. Rev. Lett.* **50**, 1589 (1984).
20. E. D. Specht *et al.*, *J. Phys. (Paris) Lett.* **45**, L561 (1985).
21. S. E. Nagler *et al.*, *Phys. Rev. B* **32**, 7373 (1985).

22. A. N. Berker, S. Ostlund, F. A. Putnam, *Phys. Rev. B* 17, 3650 (1978); R. G. Caflisch, A. N. Berker, M. Kardar, *ibid.* 31, 4527 (1985); T. Halpin-Healy and M. Kardar, *ibid.*, p. 1664. See also D. A. Huse and M. E. Fisher, *Phys. Rev. Lett.* 49, 7931 (1982); *Phys. Rev. B* 29, 239 (1984).
23. M. Kardar and A. N. Berker, *Phys. Rev. Lett.* 48, 1552 (1982).
24. E. D. Specht, M. Sutton, R. J. Birgeneau, D. E. Moncton, P. M. Horn, *Phys. Rev. B* 30, 1589 (1984).
25. D. E. Moncton, P. W. Stephens, R. J. Birgeneau, P. M. Horn, G. S. Brown, *Phys. Rev. Lett.* 46, 1533 (1981); *ibid.* 49, 1679 (1982).
26. P. W. Stephens *et al.*, *Phys. Rev. B* 29, 3512 (1984).
27. K. L. D'Amico *et al.*, *Phys. Rev. Lett.* 53, 2250 (1984).
28. S. N. Coppersmith, D. S. Fisher, B. I. Halperin, P. A. Lee, W. F. Brinkman, *ibid.* 46, 549 (1981); *ibid.*, p. 869; *Phys. Rev. B* 25, 349 (1982).
29. F. F. Abraham, S. W. Koch, W. E. Rudge, *Phys. Rev. Lett.* 49, 1830 (1982).
30. We thank G. S. Brown, R. Clarke, K. L. D'Amico, P. Dimon, P. A. Heiney, H. Hong, S. G. J. Mochrie, D. E. Moncton, S. E. Nagler, T. F. Rosenbaum, E. D. Specht, P. W. Stephens, and M. Sutton for stimulating interactions during the course of this research. We are especially grateful to D. E. Moncton who initiated our joint work in synchrotron radiation and who participated in many of the experiments discussed here. The work at the Massachusetts Institute of Technology was supported by the U.S. Army Research Office, the Joint Services Electronics Program, and the National Science Foundation Materials Research Laboratory.

# Safeguarding Our Military Space Systems

MICHAEL M. MAY

**The vulnerability of military space systems depends on their orbits, functions, and other characteristics. The high-altitude satellites needed for warning and communications in particular could be vulnerable to prompt destruction by certain space-based systems and, in the future, possibly by ground-based high power lasers. A combination of passive countermeasures and arms control agreements could give these satellites some protection against such attack. Deployment of strategic defensive systems with the capability to reach far into space would invalidate this approach.**

THE MEASURES THAT CAN BE TAKEN TO SAFEGUARD OUR military space systems or the functions carried out by these assets, the potential effectiveness of the measures, and the utility of arms control agreements vary according to the function to be safeguarded. Broad statements, arguing that space assets are few and fragile or that the deployment of antisatellite systems (ASAT's) is unverifiable, do not usefully summarize what can or cannot be done.

Military space systems consist of satellites, earth stations, and links between them (Fig. 1). The characteristics that mainly affect the vulnerability of these systems, such as altitudes of orbits, nature of components, and the like are discussed in the first part of this article. Then various ways of attacking the systems along with steps that can be taken to counter the attack or make it less effective are described. Next, the adequacy of these steps in safeguarding some space system functions are evaluated, mainly to illustrate the kind of analysis that must be done in each case. Finally, the potential value of some arms control agreements in further safeguarding these functions is discussed.

## Vulnerability of Military Space Systems

Space systems can be used for surveillance of either strategic assets or tactical situations, for warning, for communication, for weather information, for navigation, and for targeting. Figure 2 displays typical orbits for these various kinds of missions. The orbit is the main determinant of vulnerability. It determines the time and cost for an earth-launched ASAT to get to the satellite, as well as the power needed for a laser or particle beam to destroy a satellite. Warning and communication satellites are typically in very high orbits. Surveillance, weather, and targeting satellites, which need to see details on the surface of the earth, will typically be in lower orbits—how low depends on the scale of the details needed and on the resolving power of the optics. Radar surveillance and navigation satellites can be in intermediate orbits.

Several kinds of componentry might go into the various kinds of satellites (Fig. 3): transponders used for communication, radar antennas, solar power panels, and internal electronics. Not all componentry would be on any one satellite, and there are other kinds. The ones shown in Fig. 3 are all necessary for some satellites. They illustrate the range of vulnerabilities that can be expected from most componentry.

Vulnerability can be due to material damage, blinding or jamming of sensors, or damage or false signals induced in the electronics. Let me take up material damage first. Some of the materials used on satellites that were designed without special attention to hardening can be quite fragile. Normal solar panels, for instance, will fail at relatively low levels of laser or nuclear irradiation. With special attention to the materials and design, however, the material problem can be solved to the point that a satellite can only be destroyed by either (i) a direct hit, (ii) a nuclear explosion sufficiently close that it can destroy only that satellite and no other (*1*), or (iii) laser irradiation at levels than can be delivered only by sizable, costly facilities designed and tested for the purpose.

The blinding or jamming of sensors must be done by radar, infrared, or visible light sources according to the frequency band the sensor operates in. Such "in-band" jamming can be countered by rapidly changing the frequency at which the radar operates, by rapidly shuttering the optical elements of a camera, or by other measures. One particular countermeasure applies to infrared sensors. For launch warning purposes these sensors need only pick up

M. M. May is associate director at large at the Lawrence Livermore National Laboratory, Livermore, CA 94550. This article is adapted from a paper he presented at the summer workshop of the Aspen Strategy Group held in Aspen, CO, on 13 August 1985.